MGG-Net: A Multi-Modal Feature Extraction and Global-Aware Feature Graph-Based Deep Learning Network for MGMT Status Classification in Glioma

Haoyang Liu[1][0009−0006−4634−779X], Yuwen Zeng[1][0000−0003−3615−7766], Xiaoyong Zhang[2], Wentong Zhou[1], Arata Nagai[1], Masayuki Kanamori[1], Hidenori Endo[1], and Noriyasu Homma[1] ⋆

[1] Tohoku University, Japan
[2] National Institute of Technology, Sendai College.
liu.haoyang.r4@dc.tohoku.ac.jp

Abstract. Gliomas, especially high-grade gliomas, have a high mortality rate. O6-Methylguanine-DNA Methyltransferase (MGMT) status is crucial for gliomas treatment and prognosis. Traditional diagnosis relies on invasive tissue analysis, which is often infeasible for high-risk patients. While machine learning and deep learning methods using multi-sequence Magnetic Resonance Imaging (MRI) images and radiomics provides a non-invasive alternative, existing methods suffer from low accuracy and poor generalization due to challenges in extracting features from the integrated multi-sequence representation. To address this issue, we propose a Multi-modal feature extraction and Global-aware feature Graph-based deep learning network (MGG-Net), integrating convolutional neural network (CNN) and graph convolutional network (GCN) for multi-modal and multi-scale feature learning. Specifically, MGG-Net consists of multiple CNN-GCN stages, responsible for processing MRI image features and radiomic features at different scales. CNN blocks are used to extract fine-grained and sequence-specific local features from each MRI sequence. These features are then fed into a GCN, which models long-range dependencies and extracts high-level global representations. Finally, the fused multi-scale features extracted are used for classification. Experimental results demonstrate that MGG-Net outperforms previous approaches, effectively leveraging multi-scale and multi-modal information for improved MGMT status classification.

Keywords: Deep learning · Graph convolutional network · Glioma · Multi-sequence MRI.

1 Introduction

Gliomas [1] are primary brain tumors derived from neural glial stem or progenitor cells. Among them, World Health Organization (WHO) grade IV glioblas-

⋆ homma@tohoku.ac.jp

toma (GBM) is highly malignant [2]. A crucial prognostic biomarker, O6-methylguanine-DNA methyltransferase (MGMT), plays a key role in treatment response—its methylation-positive status suppresses gene expression [3], increasing sensitivity to temozolomide therapy [4]. Thus, MGMT methylation testing is essential for clinical decision-making. However, current detection methods require tissue samples obtained through surgery or biopsy, posing significant risks. Therefore, a safe and effective non-invasive detection strategy is urgently needed.

Multi-sequence magnetic resonance imaging (MRI) [5] and radiomics [6] offer non-invasive methods for MGMT status diagnosed by capturing tumor anatomy and function. Multi-sequence MRI provides structural and physiological details, while radiomics extracts high-throughput features reflecting tumor heterogeneity. Although multi-sqeuenced MRI and radiomics have been widely explored, existing methods struggle to fully utilize complementary information. Prior studies fall into machine learning and deep learning approaches. Machine learning [7–9] relies on handcrafted features, limiting scalability and adaptability. Deep learning, including convolution neural networks (CNNs) [10–12] and Transformers [13], address these issues but have their own limitations. CNNs process images as structured grids, enabling the extraction of single-sequence MRI features but struggling to capture fused-sequence MRI representations [14]. Transformers process images as linear sequences, computing token similarities. However, different MRI sequences, despite representing the same medical entity, may encode information differently, making multi-modal fusion challenging. These limitations highlight the need for a more effective fusion strategy.

To address these limitations, we propose a Multi-Modal Feature Extraction and Global-Aware Feature Graph-Based Deep Learning Network (MGG-Net). MGG-Net consists of two key components: Multi-modal Feature Extraction (MFE) and Global-Aware Feature Graph (GAFG). The MFE module leverages CNNs to extract features from individual MRI sequences, overcoming the limitation of CNNs in capturing fused sequence representations. Meanwhile, the GAFG module employs graph convolutional networks (GCNs) [15] to construct adaptive feature graphs that encode spatial relationships and intra-tumor dependencies. Unlike Transformers, which compute token similarities in a fixed sequence, GAFG dynamically models relationships between MRI sequences, adapting to their differing information representations. By integrating CNN-driven local feature extraction with GCN-based global aggregation, MGG-Net effectively addresses the fusion challenges faced by prior methods. This dynamic feature refinement across graph nodes enhances cross-modality interactions and intra-tumor feature propagation, allowing the model to focus on the most informative tumor regions, such as necrotic cores, which are crucial for MGMT status classification. Ultimately, MGG-Net overcomes the rigid grid constraints of CNNs and the limitations of sequence-based modeling in Transformers, leading to improved classification performance.

Our main contributions are summarized as follows:

– In each MFE module, we process the four MRI sequence separately and incorporate their radiomic features, capturing local representations at each scale before downsampling for the next stage.
– The GAFG module applies dynamic axial graph convolution at each scale to aggregate global contextual relationships, ultimately providing a novel and non-invasive approach for MGMT status classification.

2 Methodology

This study proposes MGG-Net, as shown in Figure 1 consisting of MFE and GAFG modules. The MFE module extracts local information by independently processing four MRI sequences (T1c, FLAIR, DWI, SWI) using feature extractor and integrating radiomic features for each sequence. The extracted sequence-specific features are passed to the GAFG module, where they are further integrated to capture inter-modality dependencies. MGG-net adopts a multi-scale architecture with four cascaded stages, where features are progressively refined. Finally, Global Average Pooling (GAP) fuses multi-scale features, and a lightweight 3D convolution serves as the MGMT classification head, determining whether MGMT is methylated.

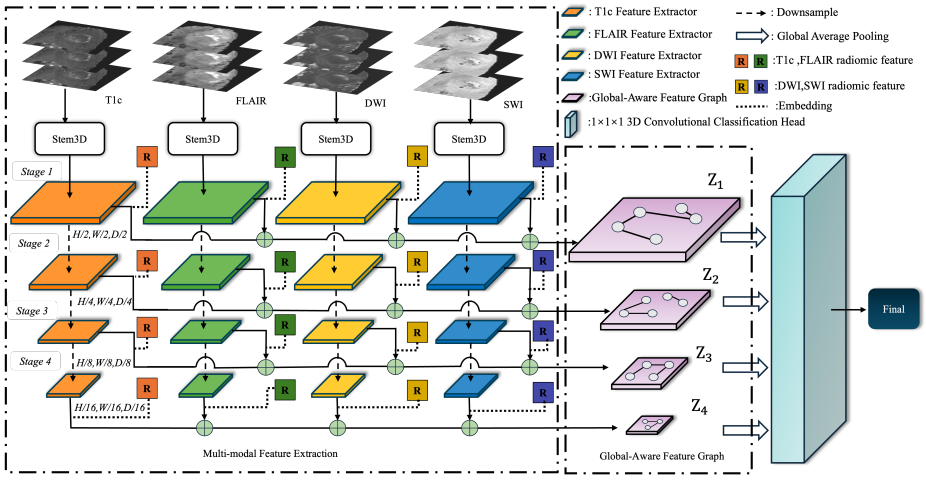

Fig. 1: The MGG-Net framework consists of the Multi-modal Feature Extraction (MFE) and Global-Aware Feature Graph (GAFG) modules. MRI sequences (T1c, FLAIR, DWI, SWI) are processed independently, with radiomic features embedded into each sequence at every stage. Extracted features are fused and structured into a graph to model inter-modal and spatial relationships, enabling MGMT classification.

2.1 Multi-modal Feature Extraction (MFE)

The MFE module consists of four parallel Feature Extraction Streams, each processing one MRI sequence (T1c, FLAIR, DWI, SWI). As shown in Figure 2, (a) illustrates 3D stem layer (Stem3D) used for initial feature extraction, while (c) presents the Feature Extractor. The feature extractor consists of a Depthwise Separable 3D Convolution (DWSConv) [16] for local feature extraction and an Inverted Residual (IR) connection for feature refinement. Given an input MRI volume $\mathbf{X}_m \in \mathbb{R}^{C_{\text{in}} \times H \times W \times D}$, where m denotes different MRI sequences, Stem3D extracts preliminary features and downsamples the input, producing $\mathbf{X}'_m$. This is then processed by DWSConv, which sequentially applies pointwise, depthwise, and pointwise convolutions. A pointwise convolution $\mathbf{W}_1 \in \mathbb{R}^{1 \times 1 \times 1 \times C_{\text{in}} \times C_{\text{mid}}}$ expands the channel dimension, followed by batch normalization and GeLU activation. A depthwise convolution $\mathbf{W}_d \in \mathbb{R}^{K \times K \times K \times C_{\text{mid}}}$ captures spatial features while maintaining channel independence. Finally, another pointwise convolution $\mathbf{W}_2 \in \mathbb{R}^{1 \times 1 \times 1 \times C_{\text{mid}} \times C_{\text{out}}}$ reduces the channel dimension, followed by batch normalization. The IR connection adds the Stem3D output directly to the stage final result, refining features while preserving spatial consistency.

At the end of each MFE stream, the radiomic features $\mathbf{R}_m \in \mathbb{R}^{B \times C_r}$,which are directly extracted from the tumor regions in the original images, are projected into an embedding space and then transmitted to match the spatial dimensions of $\mathbf{Y}_m$. Specifically, a sequence-specific transformation layer, MLP_m, maps $\mathbf{R}_m$ to $\mathbb{R}^{B \times C_{\text{mid}}}$. The resulting features are then expanded along spatial dimensions to $\mathbb{R}^{B \times C_{\text{mid}} \times D \times H \times W}$ to ensure compatibility with $\mathbf{Y}_m$. Finally, the expanded radiomic features are combined with $\mathbf{Y}_m$ via element-wise addition, producing the stage final feature map $\mathbf{Z}_m$.

After feature extraction, spatial resolution is progressively reduced, allowing the network to capture high-level representations. The extracted individual feature maps from all four sequences are then fused into a integrated representation and processed by the Global-Aware Feature Graph (GAFG) module.

2.2 Global-Aware Feature Graph (GAFG)

The GAFG module, focuses on capturing long-range dependencies by modeling global spatial relationships in the fused multi-modal feature representation, as shown in Figure 2 (c). First, a fusion layer concatenates the four individual feature maps from the MFE module along the channel dimension and applies a $1 \times 1 \times 1$ convolution. Next, a depthwise $5 \times 5 \times 5$ conditional position encoding (CPE) integrates positional information by convolving and then adding the original features back. To preserve the initial fused representation, a residual connection is introduced, where the input to CPE is added back to the final output.

The position-aware feature is then passed to the dynamic axial graph convolution network (DA-GCN). To estimate the overall mean and standard deviation of the position-aware feature, it is first divided into eight quadrants. The L_1 distances between corresponding voxels in diagonally opposite quadrants are

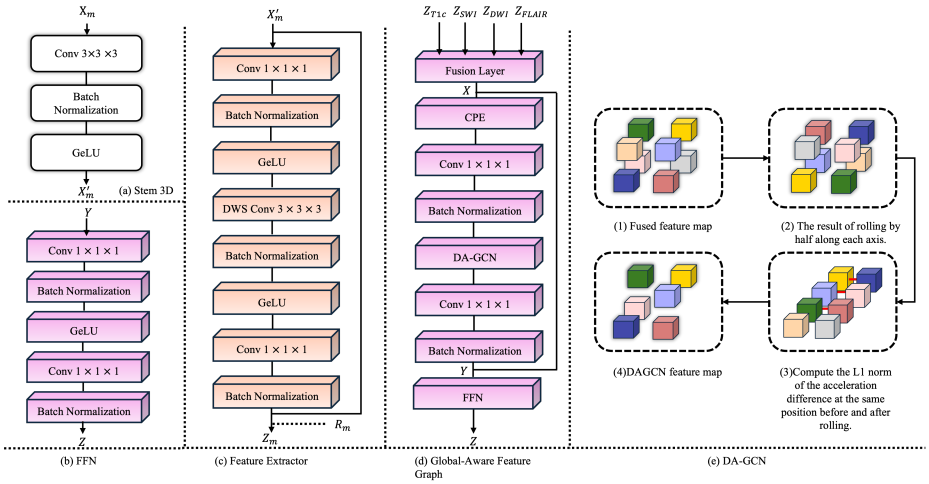

Fig. 2: Detailed structure of MFE and GAFG. (a) illustrates Stem3D, which performs preliminary feature extraction on MRI images. (b) presents the structure of the final FFN layer in GAFG. (c) shows the feature extractor structure for the four MRI sequences, incorporating radiomic features at the final step. (d) depicts the architecture of GAFG. (e) demonstrates the workflow of DA-GCN using an example where the image is rolled by half of its depth, height, and width.

computed, forming a distance distribution. The mean and standard deviation of this distribution are then used as an approximation for the global statistics of the position-aware feature. Following this, a rolling operation is performed along the depth, height, and width dimensions based on the predefined K value. As illustrated in Figure 2(e), when K is set to half of the depth, height, and width, the rolling process of DA-GCN is demonstrated. The L_1 distances between voxel pairs before and after rolling are computed. If the distance falls within the range of mean $\pm$ standard deviation, the two voxels are considered to share information, and an edge is constructed between them. As shown in Figure 3, the application of DA-GCN enables a more precise extraction of the necrotic tumor region compared to CNN-based methods, demonstrating its effectiveness in capturing tumor-specific features.

Finally, as shown in Figure 2 (b), a feed-forward network (FFN) refines $\mathbf{Y}$ via a channel-expansion and reduction process, combined with residual connections and layer scaling. This process produces the output $\mathbf{Z}$, which represents the output of Stage 1. The MFE-GAFG consists of four stages, as shown in Figure 1 each generating a $\mathbf{Z}$ with progressively smaller spatial dimensions and increasing feature dimensions. These four $\mathbf{Z}$ representations are then stacked along the channel dimension and passed through an MGMT classification head followed by a softmax layer, producing the final probability values for MGMT methylated and unmethylated status.

3 Experiment and Result

3.1 Dataset and Implementation details

This study uses the UCSF-PDGM dataset [17], which includes 501 glioma patients with standardized 3T multi-sequence MRI scans (T1, T1c, T2, FLAIR, DWI, SWI), tumor segmentation labels, and genetic data (IDH, MGMT). We focused on WHO grade IV cases [18], selecting 367 patients with enhancing tumor, necrotic tumor, and edema regions based on segmentation and MGMT status (positive/negative). Based on experimental results, we identified T1c, FLAIR, SWI, and DWI as the most informative MRI sequence for MGMT status classification. The dataset was split 0.85:0.15 for training and testing, with four-fold cross-validation. Tumor regions were extracted and cropped to 128×128×128. PyRadiomics [19] was then used to extract radiomic features, and ANOVA selected the four most relevant features per region for MGMT prediction.

Our MGG-Net was trained on an NVIDIA RTX A6000 GPU. We employed weighted focal loss [20] for the MGMT classification. Four-fold cross-validation was conducted, with each fold trained for 80 epochs. The learning rate used cosine annealing, decaying from 0.0002 to 0.0001. The batch size was set to 4.

3.2 Comparison with Existing Methods

We evaluate model performance using accuracy (Acc), precision (Prec), recall (Rec), F1-score (F1), and AUC [21], reported as mean ± standard deviation (SD). For comparison, we selected ResNet+SVM [11] and vViT [13], representing CNN and Transformer architectures, respectively, to evaluate MGG-Net's advantages in local feature extraction and global modeling. As shown in Table 1, MGG-Net (T1c, DWI, SWI, FLAIR) achieved the highest performance in Acc, Prec, F1, and AUC, while maintaining competitive Rec. Interestingly, traditional methods showed decreased performance when using DWI and SWI instead of T1 and T2, while MGG-Net achieved better results with DWI and SWI, highlighting its superior ability to handle low-contrast inputs.

Table 1: Performance of Different Methods Incorporating Radiomic Features (Mean ± SD)

Method	Acc (%)	Prec (%)	Rec (%)	F1 (%)	AUC (%)
ResNet+SVM (T1, T1c, T2, FLAIR)[11]	$66.07_{\pm 4.2}$	$73.67_{\pm 0.9}$	$\mathbf{81.88}_{\pm 10.0}$	$77.20_{\pm 4.6}$	$53.56_{\pm 3.8}$
ResNet+SVM (T1c, DWI, SWI, FLAIR)[11]	$61.61_{\pm 0.9}$	$70.41_{\pm 1.1}$	$80.00_{\pm 4.7}$	$74.80_{\pm 1.4}$	$45.35_{\pm 3.0}$
vViT (T1c, T2)[13]	$52.68_{\pm 2.9}$	$70.71_{\pm 3.9}$	$59.38_{\pm 11.0}$	$63.63_{\pm 5.7}$	$49.22_{\pm 6.6}$
MGG-Net (T1, T1c, T2, FLAIR)	$66.97_{\pm 2.0}$	$75.20_{\pm 2.7}$	$80.63_{\pm 3.7}$	$77.70_{\pm 12.0}$	$63.28_{\pm 3.3}$
MGG-Net (T1c, DWI, SWI, FLAIR)	$\mathbf{72.33}_{\pm 5.1}$	$\mathbf{81.50}_{\pm 2.9}$	$79.38_{\pm 8.4}$	$\mathbf{80.18}_{\pm 4.5}$	$\mathbf{69.02}_{\pm 2.2}$

Previous studies commonly used T1, T1c, T2, FLAIR, and radiomics for glioma analysis. We hypothesized that replacing T1 and T2 with DWI and SWI

could better capture tumor cellularity, necrosis, and vascular features [22], enhancing classification. To validate this, we compared both sequence sets across methods. Results confirmed our hypothesis: MGG-Net performed more robustly than the baselines, especially when using DWI and SWI. The contrast between ResNet+SVM's performance drop and MGG-Net's improvement suggests that the MFE module extracts more informative features from low-contrast images, and the GAFG module effectively fuses global multi-sequence information. While the improvement of MGG-Net across sequence sets was modest, its relative gain over traditional methods was substantial.

3.3 Ablation Study on MGG-Net

To gain deeper insights into the impact of different MRI sequence combinations on MGMT status classification, we conducted an ablation study, as shown in Table 2. Previous study [11] has shown that using a single T1 sequence can achieve higher classification accuracy compared to certain multi-modal combinations. However, our ablation results demonstrate that integrating multiple sequences, particularly T1c, FLAIR, SWI, and DWI, enhances classification performance. The best performance was achieved using these four MRI sequences along with radiomics features, yielding 72.3±5.1% accuracy, 81.5±2.9% precision, 80.2±4.5% F1-score, and the highest AUC of 69.0±2.2%. Notably, the inclusion of SWI and DWI significantly improved the results, as SWI provides insights into tumor angiogenesis and necrosis, while DWI reflects tumor cellularity and microstructural changes, both of which are critical for glioblastoma characterization. These findings suggest that while a single T1 sequence may perform well in certain cases, leveraging complementary information from multiple modalities leads to a more robust MGMT classification model.

Table 2: Performance of Different MRI Sequence Combinations (Mean ± SD)

T1c	FLAIR	SWI	DWI	T1	T2	Radiomics	Acc (%)	Prec (%)	Rec (%)	F1 (%)	AUC (%)
✓	✓			✓	✓	✓	$66.97_{\pm 2.0}$	$75.20_{\pm 2.7}$	$80.63_{\pm 3.7}$	$77.70_{\pm 12.0}$	$63.3_{\pm 3.3}$
✓	✓	✓	✓				$68.75_{\pm 3.2}$	$74.58_{\pm 2.4}$	$\mathbf{85.63}_{\pm 5.4}$	$79.59_{\pm 2.5}$	$63.01_{\pm 4.2}$
✓						✓	$60.27_{\pm 2.9}$	$72.01_{\pm 1.2}$	$72.50_{\pm 4.3}$	$72.2_{\pm 2.7}$	$44.49_{\pm 7.1}$
✓	✓	✓	✓			✓	$\mathbf{72.33}_{\pm 5.1}$	$\mathbf{81.50}_{\pm 2.9}$	$79.38_{\pm 8.4}$	$\mathbf{80.18}_{\pm 4.5}$	$\mathbf{69.02}_{\pm 2.2}$

Additionally, we compared our MGG-Net with MGC-Net, which replaces the graph module with a CNN [23] (Table 3). MGG-Net achieved higher accuracy and AUC, demonstrating its superiority in capturing tumor spatial relationships on multi-modal feature maps. These results confirm the advantage of integrating graph-based learning for MGMT status classification.

Because some classification models [24, 25] yield correct results without focusing on key regions, we visualized feature maps to analyze the mechanisms

Table 3: Replacing Graph Module with CNN (Mean ± SD)

Model	Acc (%)	Prec (%)	Rec (%)	F1 (%)	AUC (%)
MGG-Net	**72.33**$_{\pm 5.1}$	**81.50**$_{\pm 2.9}$	79.38$_{\pm 8.4}$	**80.18**$_{\pm 4.5}$	**69.02**$_{\pm 2.2}$
MGC-Net	70.54$_{\pm 4.5}$	78.42$_{\pm 4.4}$	**81.88**$_{\pm 8.5}$	79.71$_{\pm 3.7}$	68.26$_{\pm 4.9}$

behind performance gains. Figure 3 presents feature maps of two test cases. It is evident that the most discriminative features are concentrated in the necrotic core of the tumor, which aligns with the superior classification performance achieved when incorporating DWI and SWI. These sequences capture essential tumor characteristics, such as cellular density and vascular abnormalities, which are critical to predicting the status of MGMT. Furthermore, the GAFG-based representation exhibits a more focused activation compared to the CNN-based approach, demonstrating that the graph-based method more effectively captures key tumor features. This further supports the advantage of our multi-sequence MRI fusion strategy in improving classification accuracy.

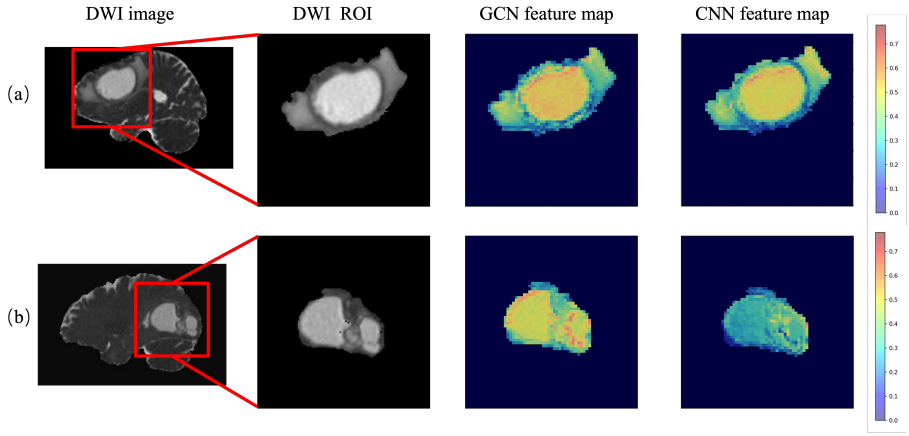

Fig. 3: Visualization results of classification feature maps using Graph and CNN-based methods. Rows (a) and (b) correspond to two patients from the test set. The "DWI image" column presents the tumor structure of each patient, while the "DWI ROI" column highlights the tumor region. The "GCN feature map" and "CNN feature map" columns show the extracted feature maps of the tumor region using the Graph and CNN-based methods, respectively. The red-highlighted areas indicate the key regions of interest for the models.

4 Conclusion

In this study, we propose MGG-Net, a novel network for multi-sequence MRI and radiomic features processing that leverages GCNs to enhance global feature extraction. By integrating multi-scale features, the model effectively utilizes diverse imaging sequences, particularly DWI and SWI, which provide crucial information on tumor cellularity and necrosis, improving MGMT status classification. Although the limited radiomic features used may restrict significant performance improvements, future work will explore enhanced fusion methods. Feature visualization confirms that MGG-Net prioritizes key tumor subregions, strengthening its effectiveness in glioblastoma analysis and highlighting the potential of graph-based learning for medical image classification.

Acknowledgments. This study was supported by the AMED No. 24ym0126812j0003 and the JSPS KAKENHI Grant Number JP25K21579.

Disclosure of Interests. The authors have no competing interests to declare that are relevant to the content of this article.

References

1. Weller, M., Wick, W., Aldape, K., Brada: Glioma. Nature reviews Disease primers **1**(1), 1–18 (2015)
2. Louis, D.N., Perry, A., Wesseling, P.: The 2021 who classification of tumors of the central nervous system: a summary. Neuro-oncology **23**(8), 1231–1251 (2021)
3. Gibson, D., Vo, A.H., Lambing, H., Bhattacharya, P., Tahir, P., Chehab, F.F.: A systematic review of high impact cpg sites and regions for mgmt methylation in glioblastoma [a systematic review of mgmt methylation in gbm]. BMC neurology **24**(1), 103 (2024)
4. Wick, W., Weller, M., Van Den Bent, M.: Mgmt testing—the challenges for biomarker-based glioma treatment. Nature Reviews Neurology **10**(7), 372–385 (2014)
5. Mabray, M.C., Barajas Jr, R.F., Cha, S.: Modern brain tumor imaging. Brain tumor research and treatment **3**(1), 8 (2015)
6. Chaddad, A., Kucharczyk, M.J., Daniel, P., Sabri, S., Jean-Claude, B.J., Niazi, T.: Radiomics in glioblastoma: current status and challenges facing clinical implementation. Frontiers in oncology **9**, 374 (2019)
7. Pálsson, S., Cerri, S., Van Leemput, K.: Prediction of mgmt methylation status of glioblastoma using radiomics and latent space shape features. In: International MICCAI Brainlesion Workshop. pp. 222–231. Springer (2021)
8. Kawaguchi, R.K., Takahashi, M., Miyake, M.: Assessing versatile machine learning models for glioma radiogenomic studies across hospitals. Cancers **13**(14), 3611 (2021)
9. Lu, Y., Patel, M., Natarajan, K.: Machine learning-based radiomic, clinical and semantic feature analysis for predicting overall survival and mgmt promoter methylation status in patients with glioblastoma. Magnetic resonance imaging **74**, 161–170 (2020)

10. Saeed, N., Hardan, S., Abutalip, K., Yaqub, M.: Is it possible to predict mgmt promoter methylation from brain tumor mri scans using deep learning models? In: International Conference on Medical Imaging with Deep Learning. pp. 1005–1018. PMLR (2022)
11. Saxena, S., Jena, B., Mohapatra, B., Gupta, N.: Fused deep learning paradigm for the prediction of o6-methylguanine-dna methyltransferase genotype in glioblastoma patients: a neuro-oncological investigation. Computers in Biology and Medicine **153**, 106492 (2023)
12. Tang, Z., Xu, Y., Jin, L., Aibaidula, A.: Deep learning of imaging phenotype and genotype for predicting overall survival time of glioblastoma patients. IEEE transactions on medical imaging **39**(6), 2100–2109 (2020)
13. Usuzaki, T., Takahashi, K., Inamori, R., Morishita, Y.: Identifying key factors for predicting o6-methylguanine-dna methyltransferase status in adult patients with diffuse glioma: A multimodal analysis of demographics, radiomics, and mri by variable vision transformer. Neuroradiology **66**(5), 761–773 (2024)
14. Ramachandran, P., Parmar, N., Vaswani, A., Bello, I., Levskaya, A., Shlens, J.: Stand-alone self-attention in vision models. Advances in neural information processing systems **32** (2019)
15. Han, K., Wang, Y., Guo, J., Tang, Y., Wu, E.: Vision gnn: An image is worth graph of nodes. Advances in neural information processing systems **35**, 8291–8303 (2022)
16. Howard, A.G., Zhu, M., Chen, B., Kalenichenko, D., Wang, W., Weyand, T.: Mobilenets: Efficient convolutional neural networks for mobile vision applications (2017), https://arxiv.org/abs/1704.04861
17. Calabrese, E., Villanueva-Meyer, J.E., Rudie, J.D.: The university of california san francisco preoperative diffuse glioma mri dataset. Radiology: Artificial Intelligence **4**(6), e220058 (2022)
18. Whitfield, B.T., Huse, J.T.: Classification of adult-type diffuse gliomas: impact of the world health organization 2021 update. Brain pathology **32**(4), e13062 (2022)
19. Van Griethuysen, J.J., Fedorov, A., Parmar, C., Hosny, A., Aucoin, N., Narayan, V.: Computational radiomics system to decode the radiographic phenotype. Cancer research **77**(21), e104–e107 (2017)
20. Lin, T.Y., Goyal, P., Girshick, R., He, K., Dollár, P.: Focal loss for dense object detection. In: Proceedings of the IEEE international conference on computer vision. pp. 2980–2988 (2017)
21. Powers, D.M.: Evaluation: from precision, recall and f-measure to roc, informedness, markedness and correlation. arXiv preprint arXiv:2010.16061 (2020)
22. Yang, X., Hu, C., Xing, Z., Lin, Y., Su, Y., Wang, X.: Prediction of ki-67 labeling index, atrx mutation, and mgmt promoter methylation status in idh-mutant astrocytoma by morphological mri, swi, dwi, and dsc-pwi. European Radiology **33**(10), 7003–7014 (2023)
23. Krizhevsky, A., Sutskever, I., Hinton, G.E.: Imagenet classification with deep convolutional neural networks. Advances in neural information processing systems **25** (2012)
24. Zeng, Y., Zhang, X., Wang, J., Usui, A., Ichiji, K., Bukovsky, I.: Inconsistency between human observation and deep learning models: assessing validity of postmortem computed tomography diagnosis of drowning. Journal of imaging informatics in medicine **37**(3), 1–10 (2024)
25. Zhang, Z., Zhang, X., Ichiji, K., Bukovskỳ, I., Homma, N.: How intra-source imbalanced datasets impact the performance of deep learning for covid-19 diagnosis using chest x-ray images. Scientific Reports **13**(1), 19049 (2023)